



1
2
3
4
5
6
7
8
9
10
11
12
13
14
15
16
17
18
19
20
21
22
23
24
25
26
27
28
29
30

Thin Organic Films Unexpectedly Enhance Alcohol Uptake on Soot Analogs: Critical Implications for Aerosol Aging

Xiangrui Kong¹, Yongjian Lian², Shuai Jiang^{2*}, Jan B. C. Pettersson^{1*}

¹*Department of Chemistry and Molecular Biology, Atmospheric Science, University of Gothenburg, Gothenburg 41390, Sweden*

²*Tianjin Key Laboratory of Urban Transport Emission Research & State Environmental Protection Key Laboratory of Urban Ambient Air Particulate Matter Pollution Prevention and Control, College of Environmental Science and Engineering, Nankai University, Tianjin 300071, China*

Correspondence to: Shuai Jiang (shuaijiang@nankai.edu.cn); Jan B.C. Pettersson (janp@chem.gu.se)



1 **Abstract**

2 Organic coatings strongly influence how gases are taken up by soot particles, yet the underlying
3 kinetics are poorly understood. Environmental molecular beam experiments combined with
4 time-of-flight mass spectrometry and molecular dynamics simulations were used to examine
5 interactions between butanol clusters and graphite surfaces with thin and thick organic coatings
6 over 180 - 300 K. Bare graphite shows two desorption pathways: a fast, temperature-insensitive
7 channel and a slower channel peaking near 210 - 220 K. Thin organic coatings suppress the
8 slow pathway entirely, consistent with rapid formation of a condensed alcohol layer that
9 stabilizes surface-bound molecules. In contrast, thick organic layers enhance slow desorption
10 and shift complete release to lower temperatures, indicating reduced molecular stability on
11 corrugated organic surfaces. Analysis reveals similar activation energies and rate parameters
12 for delayed desorption on graphite and thick coatings, pointing to a shared cluster-mediated
13 mechanism. Translating these kinetics into an effective uptake framework shows that gas-
14 particle exchange shifts between kinetic retention and desorption-limited regimes depending
15 on coating structure and temperature. Simulations further demonstrate how surface
16 morphology and coating thickness control cluster adsorption, reflection, and stability.
17 Together, these findings show that thin organic films on aged soot can strongly enhance
18 retention of semi-volatile organics, while thicker organic layers promote delayed release, with
19 important implications for aerosol aging, secondary organic aerosol formation, and climate
20 effects.

21

22 **Keywords**

23 Environmental molecular beam; clusters; nopinone; butanol; coating; thermal desorption;
24 kinetics; soot aging; organic aerosols

25

26 **Synopsis**

27 Thin organic films on soot unexpectedly enhance organic vapor uptake and retention, revealing
28 how coating structure controls aerosol aging processes that affect air quality and climate.

29

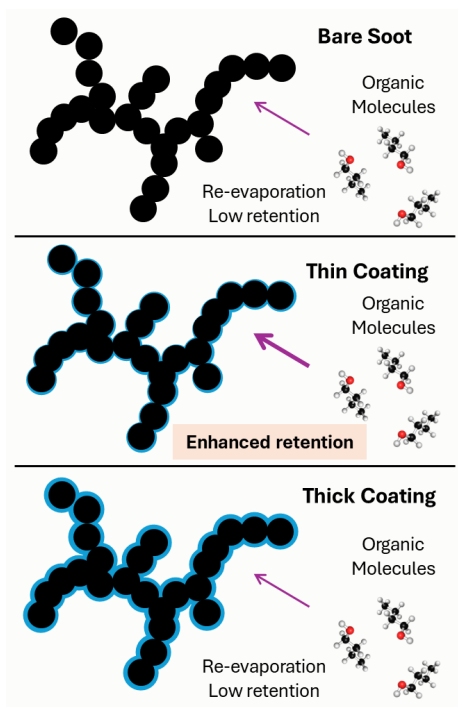
30

31

32



1 TOC graphics



2

3

4

5

6

7



1 **1. Introduction**

2 Organic coatings on atmospheric particles play a crucial role in controlling heterogeneous
3 chemistry, particle growth, and climate-relevant properties (Hallquist et al., 2009; Kroll and
4 Seinfeld, 2008). Oxygenated volatile organic compounds (OVOCs), such as short-chain
5 alcohols, are emitted from both anthropogenic and biogenic sources and readily partition
6 between the gas and particle phases (McDonald et al., 2018; Wu et al., 2020; Xia et al., 2021).
7 Once adsorbed, these molecules can undergo condensation, hydrogen bonding, or reactive
8 processing that alters aerosol composition and phase state (Shen et al., 2013). On soot particles,
9 important components of atmospheric aerosols from combustion, these processes are
10 particularly significant because soot surfaces evolve through oxidation and condensation of
11 secondary organics (Browne et al., 2015; Han et al., 2016). Such “aging” fundamentally
12 transforms soot surface chemistry, making it a dynamic interface for semi-volatile organic
13 uptake and release (Xu et al., 2020). Recent field and review work further shows that
14 coating-induced morphology changes and mixing state strongly regulate uptake, compaction,
15 and cloud condensation nuclei (CCN) activity of soot (Liu et al., 2023; Li et al., 2024).

16 Although organic coatings are widely recognized to alter soot surface properties, the molecular-
17 level mechanisms governing how coating thickness and morphology affect the accommodation
18 and desorption of semi-volatile organics remain poorly understood (Chen et al., 2020; Ahern
19 et al., 2016). Thin organic films may passivate soot surfaces, promoting stabilization of
20 condensed overlayers and suppressing molecular mobility (Omar et al., 2025). In contrast,
21 thicker organic layers can exhibit more complex morphologies, being either more corrugated
22 or smoother than thin films depending on composition and growth conditions, which alter
23 molecular packing and energy dissipation at the interface (Beeler et al., 2025). Recent
24 observations and modeling studies further demonstrate that realistic soot morphologies and
25 internal mixing states and their evolution with aging strongly influence aerosol optical and
26 climatic properties, underscoring the broader atmospheric importance of morphology-
27 dependent processes (Chen et al., 2025; Sedlacek et al., 2022). Such morphological differences
28 influence the stability, accommodation, and desorption dynamics of adsorbed species, linking
29 coating structure to the kinetic behavior of semi-volatile organics on soot (Wu et al., 2023).
30 Disentangling these contrasting effects is critical to predicting how soot and organic aerosol
31 particles exchange semi-volatile organics with the atmosphere, a process that influences
32 aerosol lifetime, reactivity, and optical properties (Berkemeier et al., 2013).

33 Previous molecular beam and temperature-programmed desorption studies have revealed that
34 alcohols interacting with graphitic surfaces exhibit multiple desorption pathways, including
35 prompt monomer release and slower desorption from cluster-bound states (Loi et al.,
36 2024; Kong et al., 2021). However, how these kinetic channels are modified by organic coatings
37 remains unresolved. The degree of coating, ranging from sub-monolayer films to micrometer-
38 thick organic layers, may determine whether volatile organics remain trapped, form condensed
39 overlayers, or desorb rapidly back to the gas phase (Ahern et al., 2016; Henögl et al., 2019).
40 Establishing this mechanistic connection between coating thickness and desorption kinetics is
41 essential for understanding the retention and reactivity of OVOCs on aged soot and organic
42 aerosols (Vaden et al., 2011).

43 In this study, we use an Environmental Molecular Beam (EMB) apparatus combined with time-
44 of-flight mass spectrometry (Kong et al., 2014b) to quantify butanol cluster interactions with
45 bare graphite, thin nopinone coatings, and nopinone thick layers under atmospherically relevant
46 temperatures (180 - 300 K). Nopinone, a monoterpene oxidation product, serves as a
47 representative organic coating compound abundant in secondary organic aerosol (Johansson
48 et al., 2020). Complementary molecular dynamics (MD) simulations are employed to resolve the



1 molecular-scale mechanisms of cluster reflection, adsorption, dissociation and desorption on
2 surfaces of varying morphology.

3 Our results show that thin organic coatings suppress slow desorption on graphite by stabilizing
4 condensed butanol overlayers, whereas thick coatings enhance delayed desorption due to
5 reduced cluster stability on the corrugated surfaces. By linking desorption kinetics with
6 molecular dynamics simulations, we demonstrate that coating thickness governs the retention
7 and release of semi-volatile organics on soot analogs, revealing how organic film morphology
8 controls alcohol uptake and reactivity during aerosol aging.

9 **2. Methodology**

10 *2.1 EMB Experiments*

11 An EMB apparatus was used to investigate the dynamics and kinetics of butanol interactions
12 with graphite and nopinone surfaces. The experimental setup, described in detail elsewhere
13 (Kong et al., 2012;Kong et al., 2014a;Johansson et al., 2017), comprises a three-chamber,
14 differentially pumped beamline. Pulsed molecular beams are generated from a gas mixture of
15 helium and butanol vapor, formed by passing helium through a liquid butanol reservoir. The
16 pulsed molecular beam, generated at 120 Hz with a 50% duty cycle, passes through a 1-mm
17 skimmer to produce a collimated, low-density flow before entering the environmental chamber.
18 The ~16 ms inter-pulse delay exceeds the residence time of fast-desorbing species, ensuring
19 that the scattering kinetics of each pulse could be observed independently (Kong et al., 2021).
20 However, in the case of the thin nopinone coating, a minor population of butanol molecules
21 with much longer residence times enables gradual buildup of a condensed butanol layer during
22 prolonged exposure.

23 The low-pressure environment ensures that observed desorption kinetics reflect intrinsic
24 surface processes rather than gas-phase diffusion, re-collision, or re-adsorption effects. While
25 atmospheric uptake occurs under ambient pressure, the same surface-controlled rate constants
26 govern gas-particle exchange and are explicitly required inputs for kinetic multilayer aerosol
27 models. The EMB approach therefore provides mechanistic and quantitative constraints on
28 interfacial processes that operate under atmospheric conditions.

29 Mass spectra show dominant peaks at $m/z = 31$ (CH_2OH^+), 41 (C_2HO^+), and 56 (C_4H_8^+) for
30 monomers, and $m/z = 75$ ($\text{C}_4\text{H}_{10}\text{OH}^+$) for clusters. A weak broad signal near $m/z = 75$ is
31 attributed to protonated cluster ions ($[\text{2 BuOH} + \text{H}]^+$), consistent with the presence of small
32 clusters (typically dominated by dimers to tetramers and with a distribution also covering larger
33 clusters) in the beam under the employed stagnation and temperature conditions. Both
34 monomers and clusters travel with an average velocity of $\sim 1600 \text{ m s}^{-1}$. The pulsed beam strikes
35 the target surface at a 45° incidence angle inside the environmental chamber, and the outgoing
36 flux is detected using a rotatable, differentially pumped quadrupole mass spectrometer (QMS)
37 for time-of-flight (TOF) analysis. Ions generated by electron impact in the QMS are collected
38 by a multi-channel scaler with a $10\text{-}\mu\text{s}$ dwell time. Highly oriented pyrolytic graphite (HOPG,
39 $12 \times 12 \text{ mm}$, grade ZYB; Advanced Ceramics Corp.) was used as the substrate and cleaned at
40 600 K before and after each experiment.

41 Nopinone surfaces were prepared by dosing vapor-phase (1R)-(+)-nopinone (98%, Sigma-
42 Aldrich) through a precision leak valve onto the substrate. The nopinone thick layer was grown
43 to a thickness of approximately $1 \mu\text{m}$. The thickness of the nopinone thick layer was determined
44 by 670 nm laser interferometry, with an estimated uncertainty of approximately $\pm 5 - 10\%$,
45 arising mainly from the refractive index of the condensed film and fringe resolution. In
46 contrast, the thin nopinone coating was below the optical detection limit of $\sim 8 \text{ nm}$ and was



1 therefore characterized using helium scattering attenuation, which provides a sensitive and
 2 reproducible measure of surface coverage (Johansson et al., 2020).
 3 The TOF distributions were analyzed to resolve the kinetics and dynamics of butanol
 4 interactions with nopinone surfaces. Upon impact, incident molecules may undergo either
 5 inelastic scattering (IS) or trapping followed by thermal desorption (TD). Incident butanol
 6 clusters are likely to trap on the surface promoted by efficient energy transfer to cluster and
 7 surface modes (Svanberg et al., 1995; Tomsic et al., 2001). A cluster may remain intact after
 8 adhering to the surface, or split into smaller cluster fragments that either remain on the surface
 9 or, with low probability, leave the surface in connection with the initial collision process
 10 (Andersson et al., 1997). Clusters that remain bound to the surface will eventually dissociate
 11 and ultimately desorb as monomers (Någård and Pettersson, 1998; Kong et al., 2021). The
 12 butanol flux from the surface is thus dominated by butanol molecules that leave the surface by
 13 either IS or TD, and both components were included in the fitting analysis. Nonlinear least-
 14 squares fitting was employed to deconvolute the IS and TD contributions. The IS component
 15 was represented by a velocity-dependent function (Arumainayagam and Madix, 1991),

$$16 \quad I_{IS}(v(t)) = C_i v(t)^4 \exp \left[- \left(\frac{v(t) - \bar{v}}{\sqrt{\frac{2k_B T_{IS}}{m}}} \right)^2 \right], \quad (1)$$

17 where C_i is a scaling parameter, v is the velocity calculated from the molecular arrival time,
 18 \bar{v} is the average velocity, k_B is the Boltzmann constant, m is the molecular mass of butanol,
 19 and T_{IS} is a free parameter representing the IS velocity spread.

20 The TD distributions are each a combination of two components: (i) a velocity distribution that
 21 relates desorption to molecular excitation based on the surface temperature,

$$22 \quad I_{TD1}(v(t)) = C_j v(t)^4 \exp \left[- \left(\frac{v(t)}{\sqrt{\frac{2k_B T_s}{m}}} \right)^2 \right], \quad (2)$$

23 and (ii) a distribution related to the desorption rates,

$$24 \quad I_{TD2} = C_j e^{-kt}, \quad (3)$$

25 where C_j is a free scaling factor, T_s is the surface temperature, k is the fitted desorption rate
 26 coefficient, and t is time. I_{TD1} shows the velocity spread of the TD flux, and I_{TD2} accounts for
 27 the exponential decay of ToF distributions. Thus, the TD distributions are calculated as a
 28 convolution of these two components. Although both IS and TD components were included in
 29 the fitting analysis, only two distinct TD channels (fast and slow) were identified and resolved
 30 from the experimental data.

31 *2.2 MD Simulations*

32 MD simulations were performed to characterize the collisions of butanol clusters with solid
 33 nopinone surfaces. The GROMOS force field, optimized for small molecules in condensed
 34 phases (Horta et al., 2016), was used to model the nopinone crystal and implemented in the
 35 GROMACS package. (Van Der Spoel et al., 2005) Molecular topologies were generated using
 36 the Automated Force Field Topology Builder (ATB) database (Malde et al., 2011; Stroet et al.,
 37 2018). Since the default ATB GROMOS charges do not reproduce melting behavior, a new set
 38 of charges was derived from *ab initio* calculations. Restrained Electrostatic Potential (RESP)
 39 point charges (Bayly et al., 1993) were fitted to replicate the electrostatic potential of an
 40 isolated nopinone molecule calculated at the BLYP-D3/6-31++G** level of theory.



1 The equations of motion were integrated using the leap-frog algorithm (Stephan et al., 2019)
2 with bond constraints applied via the LINCS method (Hess et al., 1997), allowing a 2 fs time
3 step. Short-range interactions were truncated at 1.8 nm, and long-range electrostatics were
4 treated with the particle mesh Ewald (PME) method (Essmann et al., 1995). The system
5 temperature was controlled using the velocity-rescale (V-rescale) thermostat (Bussi et al.,
6 2007) with a coupling time of 0.1 ps. The nopinone crystal structure was based on X-ray
7 diffraction data by Palin et al. (2008), obtained from the Cambridge Structural Database
8 (Groom et al., 2016).

9 An infinite crystal was generated by replicating the unit cell along all three dimensions. After
10 energy minimization with the steepest-descent algorithm, the crystal was equilibrated in the
11 NPT ensemble at 200 K for 10 ns, resulting in a simulation box containing approximately
12 100,000 atoms with dimensions $10.68 \times 16.88 \times 6.59$ nm. To model surface slabs, the crystal
13 was cleaved between nopinone bilayers to expose the most energetically favorable surface.
14 Three slabs of different thicknesses, 4 layers (~ 2.8 nm), 6 layers (~ 3.5 nm), and 15 layers (~ 9
15 nm), were prepared to represent thin and thick coatings observed experimentally. In real
16 atmospheric environments, the thickness of organic coatings on soot particles varies widely,
17 ranging from sub-nanometer patchy films on freshly emitted soot to continuous layers of tens
18 or even hundreds of nanometers on heavily aged particles (Li et al., 2024; Ahern et al.,
19 2016; Zhang et al., 2008). The simulated slab thicknesses therefore correspond to the lower end
20 of this range, representing sub-10 nm coatings typical of early soot aging under tropospheric
21 conditions. The box was extended by 10 nm in the z -direction to prevent image interactions,
22 and each slab was equilibrated in the NPT ensemble at 200 K for 10 ns.

23 Butanol clusters consisting of 10 molecules were modeled using the same GROMOS force
24 field (Horta et al., 2016) and RESP charges (Bayly et al., 1993). Stable cluster configurations
25 were first obtained from equilibrated simulations at 298 K. Cluster-surface collisions were then
26 simulated at 200 K with an incident kinetic energy of 0.45 eV (corresponding to 1606 m s^{-1})
27 and an incidence angle of 45° relative to the surface normal. Butanol clusters were decoupled
28 from the thermostat during impact to avoid artificial damping of dynamics. Initial lateral (x,y)
29 positions were randomized 1 nm above the surface, and 30 independent trajectories were
30 performed for each slab thickness to ensure statistical significance.

31 2.3 Kinetics Analysis

32 To connect the experimentally observed surface desorption kinetics to an atmosphere-relevant
33 framework, we describe gas uptake using a minimal surface-kinetic parameterization. The
34 effective uptake coefficient, γ_{eff} , is expressed as the competition between surface incorporation
35 and thermal desorption:

$$36 \quad \gamma_{\text{eff}}(T) = \alpha \frac{k_{\text{inc}}}{k_{\text{inc}} + k_{\text{des}}(T)}, \quad (4)$$

37 where α is the surface accommodation coefficient, k_{inc} is an effective incorporation rate into
38 the particle or condensed overlayer, and $k_{\text{des}}(T)$ represents the effective desorption rate of the
39 slow TD channel. The desorption rate is parameterized using an Arrhenius expression, $k_{\text{des}}(T)$
40 $= A \cdot \exp(-E_a / (k_B T))$, with effective Arrhenius parameters extracted from Figure S3 for HOPG
41 and the nopinone thick coating. These parameters represent multi-step, cluster-mediated
42 delayed desorption rather than a single elementary barrier. For the thin nopinone coating, no
43 slow TD channel is observed experimentally; therefore, no Arrhenius description is applied,
44 and this case is treated as a kinetic limit with $\gamma_{\text{eff}} \approx \alpha$. The parameter space is explored by
45 scanning temperature and incorporation timescales ($\tau_{\text{inc}} = 1/k_{\text{inc}}$), enabling regime mapping
46 without invoking detailed multilayer or diffusion-resolved models.



1 3. Results and Discussions

2 Figure 1 presents representative time-of-flight (TOF) spectra of desorbing butanol molecules
3 following cluster beam impaction on bare highly oriented pyrolytic graphite (HOPG), thin
4 nopinone coatings, and nopinone thick layers. These TOF spectra constitute the primary
5 experimental observables from which desorption dynamics and kinetic parameters are
6 extracted. The spectra illustrate the characteristic differences in desorption behavior between
7 the three surfaces at a fixed temperature and detection angle, including the presence or
8 suppression of distinct thermal desorption (TD) components. The temperature dependence and
9 relative contributions of the fast and slow TD channels, obtained from systematic analysis of
10 such TOF spectra over a range of experimental conditions, are summarized in Figures 2 and 3.
11 Additional raw TOF data recorded at different temperatures, coating thicknesses, and detection
12 angles are provided in *Supporting Information (SI)* to demonstrate the robustness and
13 reproducibility of the observed trends.

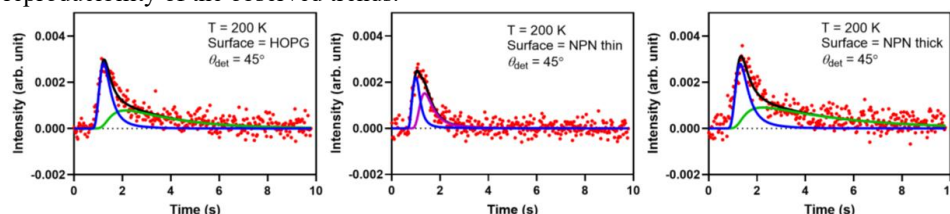


Figure 1 TOF of butanol molecule flux from HOPG, nopinone thin layer and nopinone (NPN) thick layer at 200 K, measured at 45°. Red dots represent the experimental data points. The solid lines denote nonlinear least-squares fits to the data, decomposed into fast TD (two fast TD represented by blue and purple lines, respectively) and slow TD (green lines). The thin nopinone coating exhibits only the fast TD component, indicating suppression of the slow TD channel, whereas both components are evident for HOPG and the thick layer surface.

14 3.1 Experimental Results

15 3.1.1 Interaction between butanol clusters and graphite (HOPG)

16 To establish baseline desorption behavior, the interactions of butanol clusters with HOPG were
17 examined. The TOF measurements revealed two distinct TD components: a fast channel
18 corresponding to prompt monomer release and a slow channel associated with delayed
19 desorption from cluster-bound states. The total desorbing flux exhibited a cosine angular
20 dependence, indicating that the observed signals arise exclusively from TD rather than IS
21 (Figure S1). While the incident beam contains a mixture of monomers and clusters, the
22 observed slow TD channel is attributed predominantly to the behavior of clusters upon surface
23 impact for two key reasons: (1) Monomers, due to their lower mass and fewer internal degrees
24 of freedom, are expected to undergo efficient inelastic scattering or fast TD, lacking the
25 mechanism for delayed release. (2) The kinetic model (Figure 4) and prior studies on similar
26 systems indicate that the slow TD channel originates from the dissociation and recombinative
27 desorption of clusters that have been trapped on the surface, a process not accessible to incident
28 monomers. These results confirm that butanol-graphite interactions proceed entirely via
29 thermal accommodation, providing a well-defined reference system for evaluating the effects
30 of organic coatings.

31 The temperature-dependent total flux and its decomposition into fast and slow TD components
32 are shown in Figure 2 for detection angles of 0° and 45°, defined with respect to the surface
33 normal. The total desorption intensity increases with temperature from 180 K to approximately
34 230 K and then reaches a plateau at higher temperatures, indicating that all adsorbed butanol
35 molecules have desorbed from the surface on the experimental timescale. The comparable



1 trends observed at both detection angles confirm the isotropic nature of the thermal desorption
 2 process and the absence of any nonthermal contributions.

3 The fast TD component exhibits a temperature dependence similar to that of the total flux,
 4 while the slow TD component reaches a maximum near 210-220 K. Although both desorption
 5 channels are thermally activated, the limited surface population of butanol leads to competition
 6 between them. At temperatures above ~220 K, the more efficient fast TD process depletes the
 7 surface coverage, resulting in a decline of the slow TD fraction. This depletion temperature
 8 coincides with the point where the total desorption signal levels off, confirming that all trapped
 9 butanol molecules desorb from the surface within this temperature range.

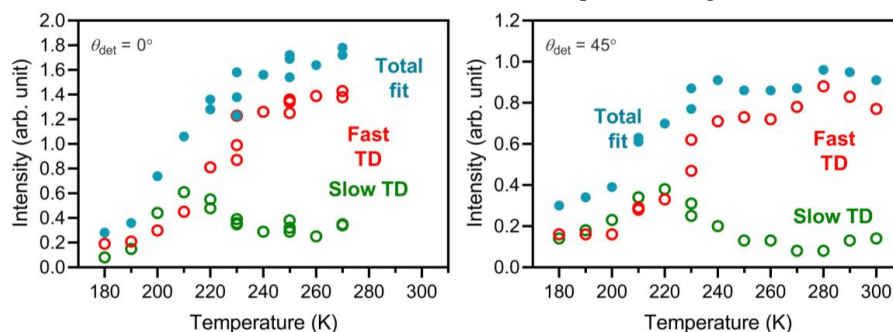


Figure 2 Temperature dependence of the total desorbing flux and its fast and slow TD components following butanol cluster impaction on HOPG.

10 **3.1.2 Constrained desorption from thin nopinone coating**

11 The TOF spectra of desorbing butanol molecules from graphite, thin nopinone coatings, and
 12 nopinone thick layers at 200 K are compared in Figure 2. The results for the thin nopinone
 13 coating exhibit a markedly shorter desorption tail relative to bare graphite, indicating the
 14 absence of the slow TD channel. In contrast, the thick layer spectrum closely resembles that of
 15 graphite, with both fast and slow TD components present. These results demonstrate that the
 16 thin coating effectively suppresses delayed desorption, implying rapid accommodation and
 17 subsequent retention of butanol on the surface within the experimental timescale (~ 10 ms).

18 The temperature dependence of the two TD channels on the three surfaces is shown in Figure
 19 3. The TOF distribution for the thin nopinone coating (Figure 2) is markedly narrower and is
 20 well-described by a single, fast TD component. Crucially, nonlinear least-squares fitting,
 21 which included the potential for an IS contribution, did not yield a significant IS component
 22 for any surface. This indicates that the observed signals are dominated by molecules that have
 23 thermally accommodated with the surface. The key finding for the thin coating is the complete
 24 absence of the slow TD channel, which is a prominent feature for both HOPG and the nopinone
 25 thick layer. Figure S2 presents additional TOF spectra obtained at different temperatures,
 26 demonstrating that the desorption process is insensitive to temperature.

27 This behavior suggests a distinct adsorption mechanism on the thin coating. The narrow, fast
 28 TD signal is consistent with the rapid formation of a condensed butanol overlayer. In this
 29 scenario, incident clusters efficiently dissipate their energy and merge into this overlayer, from
 30 which molecules desorb promptly and uniformly. In contrast, on HOPG and the thick layer,
 31 the broader fast TD signal and the presence of a significant slow TD component indicate more
 32 complex trapping and desorption pathways, likely involving a distribution of adsorption sites
 33 and the stabilization of cluster fragments that lead to delayed desorption.

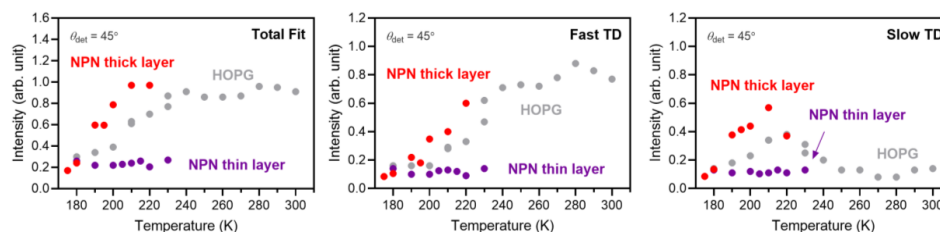


Figure 3 Temperature dependence of the total desorbing flux and its fast and slow TD components following butanol cluster impaction on HOPG, nopinone thin layer, and nopinone thick layer surfaces.

1 To confirm this mechanism, the interaction between the butanol beam and a preformed butanol
 2 coating was examined. A butanol overlayer was prepared by depositing butanol from the beam
 3 onto HOPG at temperatures below 185 K (Figure S3a). The surface coverage was monitored
 4 using helium scattering, which decreased as the surface became progressively covered by
 5 butanol. The coverage rate was higher at lower temperatures due to reduced evaporation and a
 6 constant molecular impingement rate. Consequently, at temperatures below 185 K, the
 7 desorption signal from HOPG is dominated by butanol desorption from the condensed butanol
 8 layer. The buildup of this layer was complete within tens of minutes, and TOF spectra were
 9 collected over approximately two hours. The TOF profiles from butanol-coated graphite and
 10 from the nopinone thin layer are nearly identical in both intensity and shape (Figure S3b),
 11 indicating that trapped butanol clusters readily form condensed butanol layers (analogous to
 12 those on HOPG below 185 K) but at higher temperatures when a nopinone coating is present.

13 For the nopinone thick layer, the total desorption flux is higher than that from HOPG at
 14 comparable temperatures, and complete desorption of trapped butanol occurs at a lower
 15 temperature (~210 K). The corresponding TOF spectra for the thick NPN surface are shown in
 16 Figure S4. Notably, the slow TD component (Figure 3c) is significantly enhanced on the thick
 17 layer surface, indicating that butanol clusters are less stable on the corrugated organic surface
 18 than on either HOPG or the nopinone thin layer. The mechanistic origins of the fast and slow
 19 TD channels are examined in the following kinetic analysis.

20 3.1.3 Mechanisms of fast TD and slow TD channels

21 The desorption rate constants (k) for the fast TD channel exceed the experimental time
 22 resolution and could not be quantified. Therefore, only the parameters for the slow TD process
 23 are analyzed, as presented in the Arrhenius plot in Figure 4. The analysis includes the two
 24 surfaces exhibiting slow TD behavior, HOPG and the nopinone thick layer. For HOPG, the
 25 apparent activation energy is approximately 0.12 ± 0.05 eV with a pre-exponential factor of

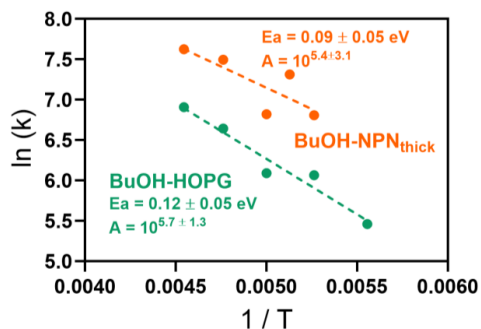


Figure 4 Arrhenius plot of butanol desorption rate constants for the slow TD channel from the nopinone thick layer surface. No data are shown for the thin nopinone coating because the slow TD channel is completely suppressed on this surface.



1 $10^{5.7 \pm 1.3} \text{ s}^{-1}$. For the nopinone thick layer, the corresponding values are $0.09 \pm 0.05 \text{ eV}$ and
 2 $10^{5.4 \pm 3.1} \text{ s}^{-1}$. Within experimental uncertainty, both systems exhibit comparable kinetic
 3 parameters, suggesting that the slow TD channels on these surfaces share a common
 4 mechanism, likely involving multiple sequential desorption processes from cluster-bound
 5 states (Kong et al., 2021; Johansson et al., 2019; Papagiannakopoulos et al., 2013).

6 The proposed kinetic scheme is illustrated in Figure 5. Upon impact with the graphite surface,
 7 butanol clusters rapidly dissociate into monomers. Owing to the weak interaction between
 8 monomers and the graphite surface, most desorb promptly, corresponding to the fast TD
 9 channel. Alternatively, some monomers can recombine with other adsorbed molecules or
 10 remaining clusters, leading to delayed desorption on a longer timescale, the slow TD channel
 11 (Kong et al., 2021). As the temperature increases, both processes accelerate; however, since
 12 the fast TD occurs directly, enhanced activity through this pathway depletes surface coverage
 13 and suppresses the slow TD contribution, consistent with experimental observations.

14 On the thin nopinone coating, the slow TD component is absent, indicating greater stabilization
 15 of adsorbed butanol. This behavior is best explained by the rapid formation of a complete
 16 butanol overlayer on the nopinone surface, which limits cluster dissociation and yields
 17 temperature-insensitive desorption kinetics. The observed fast TD signal may partly arise from
 18 direct cluster impact and energy transfer upon collision, given the high kinetic energy of the
 19 incident beam ($\sim 1 \text{ eV}$ per molecule, corresponding to a velocity of $\sim 1600 \text{ m s}^{-1}$).

20 When the nopinone forms thick layers, both the slow TD channel and temperature dependence
 21 reappear, closely resembling those observed on HOPG. The similarity in Arrhenius parameters
 22 supports a shared delayed-desorption mechanism. Notably, the slow TD channel is more
 23 pronounced for the nopinone thick layer, suggesting that the increased surface corrugation and
 24 structural heterogeneity reduce cluster stability and facilitate delayed desorption.

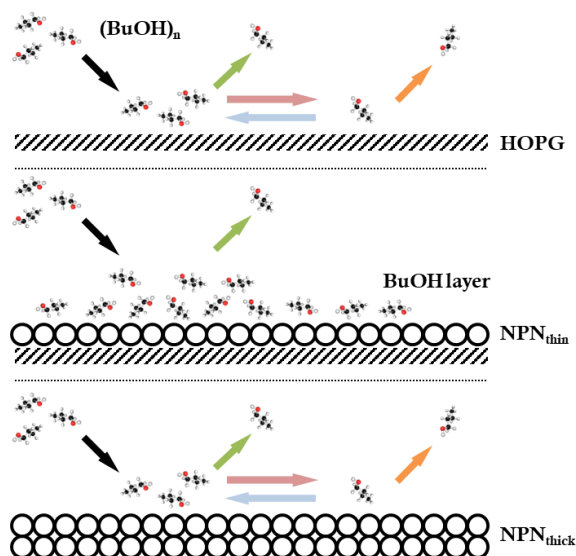


Figure 5 Schematic kinetic model illustrating butanol cluster interactions with (a) bare graphite, (b) thin nopinone coating, and (c) nopinone thick layer. Upon impact on bare graphite, clusters dissociate into monomers, producing both fast TD and slow TD via cluster-bound states. A thin nopinone coating efficiently accommodates incident clusters, stabilizing condensed butanol overlayers and suppressing the slow TD channel. In contrast, a thick nopinone layer exhibits a corrugated, crystalline surface that reduces energy accommodation, destabilizes clusters, and enhances delayed desorption.



1 3.2 Kinetic Interpretation of Uptake and Regime Mapping

2 The distinct fast and slow TD channels identified above provide a direct basis for interpreting
 3 heterogeneous uptake in kinetic terms. To translate the experimentally resolved desorption
 4 kinetics into an atmosphere-relevant description of gas-particle exchange, the effective uptake
 5 coefficient, γ_{eff} , is evaluated as the outcome of competition between surface incorporation and
 6 thermally activated delayed desorption.

7 Figure 6 illustrates how γ_{eff} transitions between kinetically controlled and desorption-limited
 8 regimes as a function of temperature and the characteristic surface incorporation timescale. In
 9 the thin-coating limit, γ_{eff} approaches the surface accommodation coefficient (α) and remains
 10 nearly temperature independent, reflecting rapid energy dissipation and efficient incorporation
 11 that suppress the slow TD channel entirely. This behavior corresponds to a kinetic retention
 12 regime in which surface residence times are sufficiently long that desorption no longer limits
 13 uptake.

14 In contrast, uptake on HOPG and on the nopinone thick layer exhibits a pronounced decrease
 15 in γ_{eff} with increasing temperature. This trend directly reflects the emergence of the slow TD
 16 channel, for which thermally activated delayed desorption increasingly competes with
 17 incorporation as temperature rises. The similar temperature dependence observed for HOPG
 18 and the thick organic layer is consistent with their comparable Arrhenius parameters and
 19 indicates a shared, desorption-controlled uptake regime.

20 These results highlight that equilibrium partitioning represents a limiting case rather than a
 21 general description of gas-particle exchange. When surface residence times are finite, uptake
 22 is governed by kinetic competition between incorporation and desorption, and coating
 23 morphology can shift particles between fundamentally different regimes. Thin organic films

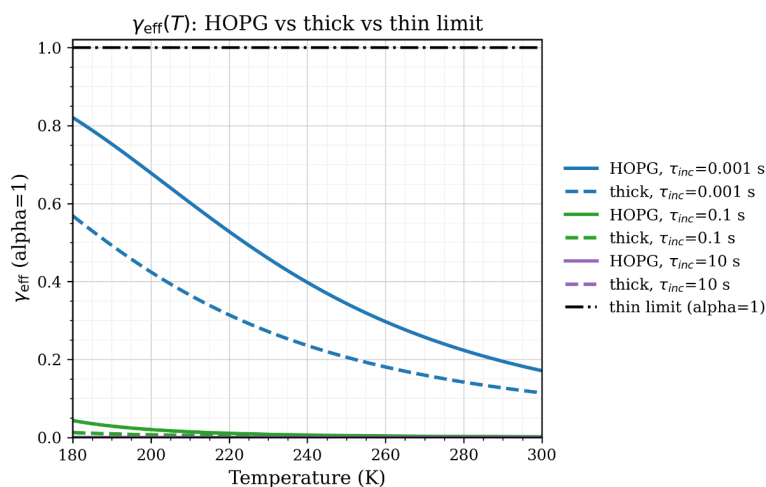


Figure 6 Temperature dependence of the effective uptake coefficient, γ_{eff} , for HOPG, a thick nopinone coating, and the thin-coating kinetic limit, evaluated at selected incorporation timescales ($\tau_{\text{inc}} = 1/k_{\text{inc}}$). The incorporation timescale represents the characteristic time required for thermally accommodated molecules or cluster fragments to be incorporated into a non-desorbing surface or near-surface environment. The scanned range of τ_{inc} ($10^{-4} - 10^3$ s) spans physically plausible limits from rapid molecular rearrangement to desorption-limited behavior and is used to identify kinetic regimes rather than to prescribe a unique atmospheric value. For HOPG and the thick coating, γ_{eff} decreases with temperature due to competition between incorporation and thermally activated slow desorption. In contrast, the thin-coating case corresponds to a kinetic limit in which no slow thermal desorption channel is observed experimentally and γ_{eff} approaches the accommodation coefficient ($\alpha = 1$).



1 promote kinetic retention by suppressing delayed desorption, whereas thicker, more ordered
2 coatings restore desorption-limited behavior. Importantly, the simple kinetic formulation
3 employed here reproduces the experimentally observed distinctions between thin and thick
4 coatings while remaining directly compatible with heterogeneous uptake parameterizations
5 used in aerosol dynamics and chemical transport models.

6 *3.3 MD Simulation Results*

7 Classical MD simulations were performed to investigate the interactions between butanol
8 clusters and nopinone surfaces. The nopinone crystal structure was constructed based on
9 experimental X-ray diffraction data (Palin et al., 2008), which reveal a bilayer arrangement in
10 which functional groups are oriented inward within each bilayer (Figure S5a). Weak van der
11 Waals forces between bilayers maintain the overall structural cohesion of the crystal. The
12 melting point of bulk nopinone is 260 K (Palin et al., 2008), and therefore, at the simulation
13 temperature of 200 K, the nopinone slabs remain crystalline.

14 Figure S5 presents simulation snapshots at key stages of a butanol cluster colliding with a 15-
15 layer nopinone slab, representing the interaction between the butanol molecular beam and a
16 nopinone surface. Initially, a 10-molecule cluster is positioned 1 nm above the surface (Figure
17 S5a). Within 15 - 30 ps of impact, one molecule reflects from the surface (Figure S5b,c), while
18 the remaining molecules divide into two fragments that adsorb onto the surface (Figure S5d,e).
19 These fragments remain bound over the next ~2 ns and reorganize into stable surface clusters
20 (Figure S5f,g). Molecules located in the cluster interior are strongly bound and resistant to
21 direct desorption, whereas those at the periphery are more weakly bound and can either desorb
22 directly or undergo a two-step process involving detachment followed by monomer desorption.

23 A non-reflective collision pathway was also observed (Figure S6b-e), in which the incident
24 cluster remains largely intact but splits into two fragments. The smaller fragment, composed
25 of three butanol molecules, is loosely bound to the nopinone surface and readily undergoes TD.
26 Both reflective and non-reflective behaviors were observed for nopinone slabs of 4-layer (~2.8
27 nm) and 6-layer (~3.5 nm) thickness. These contrasting outcomes suggest that differences in
28 surface structure may modulate cluster stability and desorption behavior, an effect examined
29 in detail below using the structural analysis in Figure 7.

30 The nopinone surface is predominantly terminated by well-ordered hydrocarbon groups,
31 rendering the carbonyl functionalities largely inaccessible to hydrogen bonding. Occasional
32 rotation of surface molecules by 180° about one of the molecular axes exposes hydroxyl groups
33 that act as surface defects, introducing localized hydrophilicity and disrupting the otherwise
34 nonpolar surface. These defect sites play a key role in mediating the adsorption and desorption
35 dynamics of impinging butanol clusters by providing transient hydrogen-bonding or dipole-
36 dipole interaction sites that enhance molecular trapping.

37 As shown in Figure 7a, the radial distribution functions (RDFs) reveal clear structural
38 differences among nopinone slabs of varying thickness. The 4-layer slab exhibits a rightward
39 shift and broadening of RDF peaks, indicative of weaker intermolecular packing and increased
40 structural disorder resembling a pre-melted or amorphous-like surface. In contrast, the 6- and
41 15-layer slabs display sharper, well-defined peaks characteristic of a solid-like crystalline
42 organization. This progressive increase in molecular order with thickness implies that thinner
43 coatings have higher densities of surface defects and greater morphological heterogeneity.

44 These structural variations translate directly into the experimentally observed desorption
45 behavior. The increased disorder and defect density in thinner coatings enhance molecular
46 accommodation, leading to efficient trapping of butanol clusters and suppression of the slow
47 TD channel. In contrast, the more ordered and corrugated surface of the nopinone thick layer

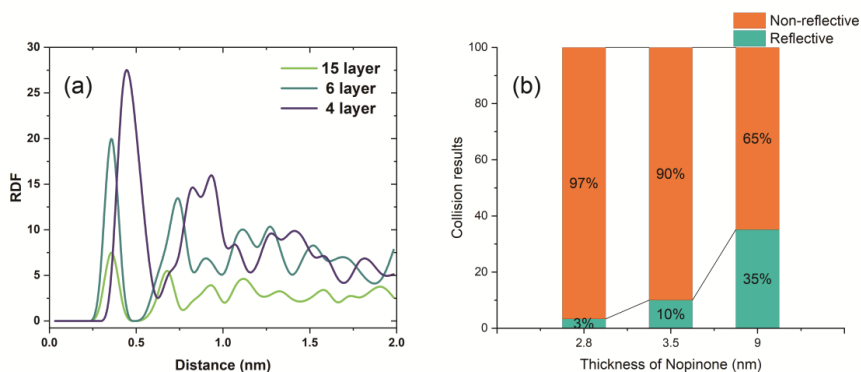


Figure 7 (a) Radial distribution functions (RDFs) calculated for the surface layer and the entire nopinone slab with thicknesses of 4 layers (~2.8 nm), 6 layers (~3.5 nm), and 15 layers (~9 nm). The RDFs were constructed using ketone group pairs as reference points. (b) The collision simulation results of thin coated nopinone (4 layers, ~2.8 nm; 6 layers, ~3.5 nm) and thick coated nopinone (15 layers, ~9 nm).

1 reduces the availability of stable adsorption sites, resulting in less efficient energy dissipation
 2 and enhanced delayed desorption, consistent with the strong slow TD signal observed
 3 experimentally.

4 Figure 7b shows that the reflection probability of butanol molecules within a cluster decreases
 5 systematically with decreasing slab thickness, confirming that disordered, defect-rich surfaces
 6 promote collisional energy loss and adsorption. Together, these simulation results provide a
 7 molecular-level explanation for the experimental findings. The thin, partially disordered
 8 nopinone coatings contain a higher density of flexible or defect sites that efficiently dissipate
 9 collisional energy and promote transient hydrogen-bonding interactions, leading to
 10 stabilization of condensed butanol overlayers. In contrast, the thicker, crystalline-like nopinone
 11 thick layers present more rigid, well-ordered hydrocarbon terminations that limit energy
 12 accommodation and reduce the availability of binding sites, thereby favoring cluster breakup
 13 and delayed desorption. The underlying graphite substrate in the thin-coating regime may
 14 further enhance adsorption by providing additional π -OH or defect-mediated interactions
 15 accessible through the incomplete nopinone layer, reinforcing the stronger retention observed
 16 experimentally.

17 4. Atmospheric Implications

18 Although the present experiments are conducted under controlled low-pressure conditions,
 19 they are designed to isolate intrinsic surface-controlled kinetic processes, such as molecular
 20 accommodation, trapping, and desorption, that govern gas-particle exchange in the atmosphere
 21 and are independent of ambient pressure. These interfacial processes occur on picosecond-to-
 22 millisecond timescales and form the mechanistic basis of kinetic aerosol models used under
 23 atmospheric conditions.

24 The present results highlight the pivotal role of organic coating thickness and morphology in
 25 governing the gas-particle exchange of semi-volatile organics and thus the dynamic evolution
 26 of atmospheric aerosols. The distinct regimes identified here, thin-film “trap-and-overlayer”
 27 versus thick-film “delayed desorption”, translate directly to processes controlling soot aging,
 28 secondary organic aerosol (SOA) growth, and cloud activation.

29 In the thin-film regime, corresponding to sub-monolayer or patchy organic coatings typical of
 30 freshly aged soot, the efficient energy accommodation and suppressed delayed desorption
 31 observed experimentally indicate that soot can act as a transient reservoir for OVOCs. Such



1 interfacial stabilization facilitates further heterogeneous oxidation and condensation, thereby
2 promoting core-shell internal mixing and soot compaction that enhance light absorption
3 (“lensing”) and modify aerosol optical properties (Lack and Cappa, 2010). The increased
4 retention of semi-volatile organics on thin films may also explain field observations of
5 extended SOA residence times and apparent equilibrium deviations under low-temperature or
6 low-humidity conditions (Vaden et al., 2011).

7 Conversely, the thick-film regime, represented by thick layer or phase-separated organic
8 coatings, exhibits enhanced delayed desorption and reduced cluster stability, behavior
9 consistent with weak energy accommodation and rapid re-evaporation. Such kinetic signatures
10 mirror the non-equilibrium partitioning and size-independent evaporation measured for viscous
11 or glassy SOA (Hallquist et al., 2009; Shiraiwa et al., 2012). In this limit, the organic surface
12 behaves more like a bulk OA phase, and delayed desorption times on the order of milliseconds
13 can be incorporated into kinetic thick layer models as effective desorption coefficients or mass
14 accommodation parameters (Berkemeier et al., 2013).

15 The morphology-dependent surface kinetics identified here also have implications for cloud
16 condensation nuclei (CCN) activity by regulating the surface residence time and mixing state
17 of semi-volatile organics on soot-containing particles. Thin organic films that efficiently
18 dissipate collisional energy and stabilize condensed, polar overlayers can promote internal
19 mixing and increase the effective hygroscopicity (κ) of soot particles, thereby enhancing CCN
20 activation (Petters and Kreidenweis, 2007). In contrast, thicker and more ordered organic
21 coatings may act as kinetic barriers to further uptake and reorganization, favoring phase-
22 separated or viscous surface states and limiting water access to the soot core (Freedman, 2017).
23 Such morphology-driven suppression of uptake is consistent with reduced κ values and partial
24 decoupling of soot from cloud activation observed for aged or phase-separated organic
25 aerosols. The coexistence of these thin- and thick-film kinetic regimes may therefore help
26 reconcile discrepancies between laboratory CCN measurements and field κ -closure for mixed
27 black carbon-organic aerosol particles.

28 At the modeling scale, these observations suggest that surface-controlled kinetic parameters,
29 rather than equilibrium partitioning constants, are required to accurately describe SVOC
30 exchange between soot and the atmosphere. Our experimentally constrained activation energies
31 (0.09 - 0.12 eV) and pre-exponential factors ($\sim 10^5 \text{ s}^{-1}$) provide realistic desorption rate
32 constants for use in kinetic thick layer frameworks and process-level models of aerosol aging
33 (Shiraiwa et al., 2012; Zaveri et al., 2014). Implementing such parameters into chemical
34 transport or climate models could improve predictions of SOA lifetime, soot mixing state, and
35 direct radiative forcing, particularly under cold and polluted conditions where organic film
36 morphology evolves rapidly.

37 Although the present study employs butanol and nopinone as model compounds, the identified
38 kinetic regimes are expected to be broadly applicable to other semi-volatile organics and
39 organic aerosol coatings. Butanol represents a prototypical oxygenated volatile organic
40 compound with moderate volatility and hydrogen-bonding capability, characteristic of many
41 alcohols and multifunctional SOA constituents, while nopinone serves as a representative
42 oxidized biogenic SOA component with limited polarity and a tendency to form ordered
43 condensed phases. The contrasting behaviors observed here arise primarily from differences in
44 coating thickness, surface disorder, and energy dissipation efficiency, rather than from the
45 specific chemical identities of the adsorbate or coating.

46 **5. Conclusions**



1 This study shows that organic coating thickness and morphology apply first-order control over
2 the surface-mediated uptake and release of semi-volatile organics on soot analogs.
3 Environmental molecular beam experiments identify two desorption pathways: a fast channel
4 associated with prompt monomer release and a slow, thermally activated channel arising from
5 cluster-bound states. Thin organic coatings suppress the slow desorption pathway by stabilizing
6 condensed overlayers, leading to a kinetic retention regime in which uptake approaches the
7 accommodation limit. In contrast, thicker and more ordered organic coatings restore delayed
8 desorption behavior similar to that on bare graphite. By translating experimentally resolved
9 desorption kinetics into an effective uptake framework, this work demonstrates that gas-
10 particle exchange is governed by kinetic competition rather than equilibrium partitioning alone.
11 Molecular dynamics simulations provide a mechanistic basis for these effects, highlighting the
12 role of surface disorder in energy dissipation and molecular trapping. Together, these results
13 establish a process-level link between organic film morphology, surface kinetics, and aerosol
14 aging.

15

16 **Acknowledgments**

17 This work was supported by the Swedish Research Council (2021-04042), the Swedish
18 Foundation for International Cooperation in Research and Higher Education (MG2022-9380),
19 and the Adlerbert Research Foundation. Additional funding was provided by the National
20 Natural Science Foundation of China (42477111), the Fundamental Research Funds for the
21 Central Universities of China (63253201), the Natural Science Foundation of Tianjin
22 Municipality (24JCYBJC01700), and the Tianjin Key Research and Development Project
23 (24YFXTHZ00070). Computational resources were provided by the National Supercomputer
24 Center in Tianjin, and calculations were performed on the Tianhe next-generation
25 supercomputer.

26

27 **Conflicts of Interest**

28 The authors declare no conflict of interest.

29

30 **Author Contributions**

31 X.K. and J.P. conceived and designed the study. X.K. performed the environmental molecular
32 beam experiments, analyzed the experimental data, and led the manuscript preparation. Y.L.
33 and S.J. performed the molecular dynamics simulations and contributed to data interpretation
34 and kinetic analysis. All authors discussed the results and contributed to the final version of the
35 manuscript.

36

37 **References**

38 Ahern, A. T., Subramanian, R., Saliba, G., Lipsky, E. M., Donahue, N. M., and Sullivan, R. C.: Effect
39 of secondary organic aerosol coating thickness on the real-time detection and characterization of
40 biomass-burning soot by two particle mass spectrometers, *Atmos. Meas. Tech.*, 9, 6117-6137,
41 10.5194/amt-9-6117-2016, 2016.



- 1 Andersson, P. U., Tomsic, A., Andersson, M. B., and Petterson, J. B. C.: Emission of small fragments
2 during water cluster collisions with a graphite surface, *Chem. Phys. Lett.*, 279, 100-106,
3 [https://doi.org/10.1016/S0009-2614\(97\)00990-1](https://doi.org/10.1016/S0009-2614(97)00990-1), 1997.
- 4 Arumainayagam, C. R., and Madix, R. J.: Molecular Beam Studies of Gas-Surface Collision Dynamics,
5 *Prog. Surf. Sci.*, 38, 1-102, 1991.
- 6 Bayly, C. I., Cieplak, P., Cornell, W., and Kollman, P. A.: A well-behaved electrostatic potential based
7 method using charge restraints for deriving atomic charges: the RESP model, *The Journal of Physical*
8 *Chemistry*, 97, 10269-10280, 10.1021/j100142a004, 1993.
- 9 Beeler, P., Corbin, J. C., Sipkens, T. A., and Fierce, L.: A Framework for Quantifying the Size and
10 Fractal Dimension of Compacting Soot Particles, *Environ Sci Technol*, 59, 5994-6003,
11 10.1021/acs.est.4c11100, 2025.
- 12 Berkemeier, T., Huisman, A. J., Ammann, M., Shiraiwa, M., Koop, T., and Pöschl, U.: Kinetic regimes
13 and limiting cases of gas uptake and heterogeneous reactions in atmospheric aerosols and clouds: a
14 general classification scheme, *Atmos. Chem. Phys.*, 13, 6663-6686, 10.5194/acp-13-6663-2013, 2013.
- 15 Browne, E. C., Franklin, J. P., Canagaratna, M. R., Massoli, P., Kirchstetter, T. W., Worsnop, D. R.,
16 Wilson, K. R., and Kroll, J. H.: Changes to the Chemical Composition of Soot from Heterogeneous
17 Oxidation Reactions, *The Journal of Physical Chemistry A*, 119, 1154-1163, 10.1021/jp511507d, 2015.
- 18 Bussi, G., Donadio, D., and Parrinello, M.: Canonical sampling through velocity rescaling, *Journal of*
19 *Chemical Physics*, 126, 10.1063/1.2408420, 2007.
- 20 Chen, C., Enekwizu, O. Y., Ma, X., Jiang, Y., Khalizov, A. F., Zheng, J., and Ma, Y.: Effect of organic
21 coatings derived from the OH-initiated oxidation of amines on soot morphology and cloud activation,
22 *Atmos Res*, 239, 104905, <https://doi.org/10.1016/j.atmosres.2020.104905>, 2020.
- 23 Chen, X., Ching, J., Wu, F., Matsui, H., Jacobson, M. Z., Zhang, F., Wang, Y., Zhang, Z., Liu, D., Zhu,
24 S., Rudich, Y., Shi, Z., Yoo, H., Jeon, K.-J., and Li, W.: Locating the missing absorption enhancement
25 due to multi-core black carbon aerosols, *Nat Commun*, 16, 10187, 10.1038/s41467-025-65079-2, 2025.
- 26 Essmann, U., Perera, L., Berkowitz, M. L., Darden, T., Lee, H., and Pedersen, L. G.: A SMOOTH
27 PARTICLE MESH EWALD METHOD, *Journal of Chemical Physics*, 103, 8577-8593,
28 10.1063/1.470117, 1995.
- 29 Freedman, M. A.: Phase separation in organic aerosol, *Chem Soc Rev*, 46, 7694-7705,
30 10.1039/C6CS00783J, 2017.
- 31 Groom, C. R., Bruno, I. J., Lightfoot, M. P., and Ward, S. C.: The Cambridge Structural Database, *Acta*
32 *Crystallographica Section B*, 72, 171-179, doi:10.1107/S2052520616003954, 2016.
- 33 Hallquist, M., Wenger, J. C., Baltensperger, U., Rudich, Y., Simpson, D., Claeys, M., Dommen, J.,
34 Donahue, N. M., George, C., Goldstein, A. H., Hamilton, J. F., Herrmann, H., Hoffmann, T., Iinuma,
35 Y., Jang, M., Jenkin, M. E., Jimenez, J. L., Kiendler-Scharr, A., Maenhaut, W., McFiggans, G., Mentel,
36 T. F., Monod, A., Prévôt, A. S. H., Seinfeld, J. H., Surratt, J. D., Szmigielski, R., and Wildt, J.: The
37 formation, properties and impact of secondary organic aerosol: current and emerging issues, *Atmos.*
38 *Chem. Phys.*, 9, 5155-5236, 10.5194/acp-9-5155-2009, 2009.
- 39 Han, C., Liu, Y., and He, H.: The photoenhanced aging process of soot by the heterogeneous
40 ozonization reaction, *Physical Chemistry Chemical Physics*, 18, 24401-24407, 10.1039/C6CP03938C,
41 2016.
- 42 Henögl, E., Haberl, V., Ablasser, J., and Schennach, R.: Adsorption and Desorption of Organic
43 Molecules From Thin Cellulose Films, *Frontiers in Materials*, Volume 6 - 2019,
44 10.3389/fmats.2019.00178, 2019.
- 45 Hess, B., Bekker, H., Berendsen, H. J. C., and Fraaije, J. G. E. M.: LINCS: A linear constraint solver
46 for molecular simulations, *J Comput Chem*, 18, 1463-1472, [https://doi.org/10.1002/\(SICI\)1096-987X\(199709\)18:12<1463::AID-JCC4>3.0.CO;2-H](https://doi.org/10.1002/(SICI)1096-987X(199709)18:12<1463::AID-JCC4>3.0.CO;2-H), 1997.



- 1 Horta, B. A. C., Merz, P. T., Fuchs, P. F. J., Dolenc, J., Riniker, S., and Hünenberger, P. H.: A
2 GROMOS-Compatible Force Field for Small Organic Molecules in the Condensed Phase: The
3 2016H66 Parameter Set, *J Chem Theory Comput*, 12, 3825-3850, 10.1021/acs.jctc.6b00187, 2016.
- 4 Johansson, S. M., Kong, X., Papagiannakopoulos, P., Thomson, E. S., and Pettersson, J. B.: A novel
5 gas-vacuum interface for environmental molecular beam studies, *Rev Sci Instrum*, 88, 035112,
6 10.1063/1.4978325, 2017.
- 7 Johansson, S. M., Lovric, J., Kong, X., Thomson, E. S., Papagiannakopoulos, P., Briquez, S., Toubin,
8 C., and Pettersson, J. B. C.: Understanding water interactions with organic surfaces: environmental
9 molecular beam and molecular dynamics studies of the water-butanol system, *Physical chemistry
10 chemical physics : PCCP*, 21, 1141-1151, 10.1039/c8cp04151b, 2019.
- 11 Johansson, S. M., Lovric, J., Kong, X., Thomson, E. S., Hallquist, M., and Pettersson, J. B. C.:
12 Experimental and Computational Study of Molecular Water Interactions with Condensed Nopinone
13 Surfaces Under Atmospherically Relevant Conditions, *J Phys Chem A*, 124, 3652-3661,
14 10.1021/acs.jpca.9b10970, 2020.
- 15 Kong, X., Andersson, P. U., Thomson, E. S., and Pettersson, J. B. C.: Ice Formation via Deposition
16 Mode Nucleation on Bare and Alcohol-Covered Graphite Surfaces, *The Journal of Physical Chemistry
17 C*, 116, 8964-8974, 10.1021/jp212235p, 2012.
- 18 Kong, X., Papagiannakopoulos, P., Thomson, E. S., Markovic, N., and Pettersson, J. B.: Water
19 accommodation and desorption kinetics on ice, *J Phys Chem A*, 118, 3973-3979, 10.1021/jp503504e,
20 2014a.
- 21 Kong, X., Thomson, E. S., Papagiannakopoulos, P., Johansson, S. M., and Pettersson, J. B.: Water
22 accommodation on ice and organic surfaces: insights from environmental molecular beam experiments,
23 *J Phys Chem B*, 118, 13378-13386, 10.1021/jp5044046, 2014b.
- 24 Kong, X., Lovrić, J., Johansson, S. M., Prisle, N. L., and Pettersson, J. B. C.: Dynamics and Sorption
25 Kinetics of Methanol Monomers and Clusters on Nopinone Surfaces, *The Journal of Physical Chemistry
26 A*, 125, 6263-6272, 10.1021/acs.jpca.1c02309, 2021.
- 27 Kroll, J. H., and Seinfeld, J. H.: Chemistry of secondary organic aerosol: Formation and evolution of
28 low-volatility organics in the atmosphere, *Atmos Environ*, 42, 3593-3624,
29 <https://doi.org/10.1016/j.atmosenv.2008.01.003>, 2008.
- 30 Lack, D. A., and Cappa, C. D.: Impact of brown and clear carbon on light absorption enhancement,
31 single scatter albedo and absorption wavelength dependence of black carbon, *Atmos. Chem. Phys.*, 10,
32 4207-4220, 10.5194/acp-10-4207-2010, 2010.
- 33 Li, W., Riemer, N., Xu, L., Wang, Y., Adachi, K., Shi, Z., Zhang, D., Zheng, Z., and Laskin, A.:
34 Microphysical properties of atmospheric soot and organic particles: measurements, modeling, and
35 impacts, *Npj Clim Atmos Sci*, 7, 65, 10.1038/s41612-024-00610-8, 2024.
- 36 Liu, Y., He, G., Chu, B., Ma, Q., and He, H.: Atmospheric heterogeneous reactions on soot: A review,
37 *Fundamental Research*, 3, 579-591, <https://doi.org/10.1016/j.fmre.2022.02.012>, 2023.
- 38 Loi, Q. K., Phothong, K., Yuasa, R., Horikawa, T., and Do, D. D.: Evidence of bimolecular layer of
39 ethanol on graphite at 190K - Experimental and simulation studies, *Carbon*, 216, 118535,
40 <https://doi.org/10.1016/j.carbon.2023.118535>, 2024.
- 41 Malde, A. K., Zuo, L., Breeze, M., Stroet, M., Poger, D., Nair, P. C., Oostenbrink, C., and Mark, A. E.:
42 An Automated Force Field Topology Builder (ATB) and Repository: Version 1.0, *J Chem Theory
43 Comput*, 7, 4026-4037, 10.1021/ct200196m, 2011.
- 44 McDonald, B. C., de Gouw, J. A., Gilman, J. B., Jathar, S. H., Akherati, A., Cappa, C. D., Jimenez, J.
45 L., Lee-Taylor, J., Hayes, P. L., McKeen, S. A., Cui, Y. Y., Kim, S.-W., Gentner, D. R., Isaacman-
46 VanWertz, G., Goldstein, A. H., Harley, R. A., Frost, G. J., Roberts, J. M., Ryerson, T. B., and Trainer,
47 M.: Volatile chemical products emerging as largest petrochemical source of urban organic emissions,
48 *Science*, 359, 760-764, 10.1126/science.aag0524, 2018.



- 1 Någård, M. B., and Pettersson, J. B. C.: Internal excitation of ethanol molecules emitted during cluster-
2 surface collisions, *Chem. Phys. Lett.*, 293, 535-540, [https://doi.org/10.1016/S0009-2614\(98\)00804-5](https://doi.org/10.1016/S0009-2614(98)00804-5),
3 1998.
- 4 Omar, H., Ahmadi, S., Szymoniak, P., and Schönhals, A.: Molecular mobility of thin films of
5 poly(bisphenol-A carbonate) capped and with one free surface: from bulk-like samples down to the
6 adsorbed layer, *Soft Matter*, 21, 241-254, 10.1039/D4SM01238K, 2025.
- 7 Palin, L., Brunelli, M., Wright, J. P., Pattison, P., and Fitch, A. N.: The low-temperature structure of
8 nopinone, 223, 602-604, doi:10.1524/zkri.2008.1101, 2008.
- 9 Papagiannakopoulos, P., Kong, X., Thomson, E. S., Marković, N., and Pettersson, J. B. C.: Surface
10 Transformations and Water Uptake on Liquid and Solid Butanol near the Melting Temperature, *The*
11 *Journal of Physical Chemistry C*, 117, 6678-6685, 10.1021/jp4003627, 2013.
- 12 Petters, M. D., and Kreidenweis, S. M.: A single parameter representation of hygroscopic growth and
13 cloud condensation nucleus activity, *Atmos. Chem. Phys.*, 7, 1961-1971, 10.5194/acp-7-1961-2007,
14 2007.
- 15 Sedlacek, A. J., III, Lewis, E. R., Onasch, T. B., Zuidema, P., Redemann, J., Jaffe, D., and Kleinman,
16 L. I.: Using the Black Carbon Particle Mixing State to Characterize the Lifecycle of Biomass Burning
17 Aerosols, *Environ Sci Technol*, 56, 14315-14325, 10.1021/acs.est.2c03851, 2022.
- 18 Shen, X., Zhao, Y., Chen, Z., and Huang, D.: Heterogeneous reactions of volatile organic compounds
19 in the atmosphere, *Atmos Environ*, 68, 297-314, <https://doi.org/10.1016/j.atmosenv.2012.11.027>, 2013.
- 20 Shiraiwa, M., Pfrang, C., Koop, T., and Pöschl, U.: Kinetic multi-layer model of gas-particle
21 interactions in aerosols and clouds (KM-GAP): linking condensation, evaporation and chemical
22 reactions of organics, oxidants and water, *Atmos. Chem. Phys.*, 12, 2777-2794, 10.5194/acp-12-2777-
23 2012, 2012.
- 24 Stephan, S., Thol, M., Vrabec, J., and Hasse, H.: Thermophysical Properties of the Lennard-Jones Fluid:
25 Database and Data Assessment, *J Chem Inf Model*, 59, 4248-4265, 10.1021/acs.jcim.9b00620, 2019.
- 26 Stroet, M., Caron, B., Visscher, K. M., Geerke, D. P., Malde, A. K., and Mark, A. E.: Automated
27 Topology Builder Version 3.0: Prediction of Solvation Free Enthalpies in Water and Hexane, *J Chem*
28 *Theory Comput*, 14, 5834-5845, 10.1021/acs.jctc.8b00768, 2018.
- 29 Svanberg, M., Marković, N., and Pettersson, J. B. C.: Energy transfer in water cluster scattering from
30 solid surfaces, *Chem Phys*, 201, 473-489, [https://doi.org/10.1016/0301-0104\(95\)00284-7](https://doi.org/10.1016/0301-0104(95)00284-7), 1995.
- 31 Tomsic, A., Andersson, P. U., Markovic, N., Piskorz, W., Svanberg, M., and Pettersson, J. B. C.:
32 Molecular-dynamics simulations of cluster-surface collisions: Emission of large fragments, *The*
33 *Journal of Chemical Physics*, 115, 10509-10517, 10.1063/1.1413740, 2001.
- 34 Vaden, T. D., Imre, D., Beránek, J., Shrivastava, M., and Zelenyuk, A.: Evaporation kinetics and phase
35 of laboratory and ambient secondary organic aerosol, *Proceedings of the National Academy of*
36 *Sciences*, 108, 2190-2195, 10.1073/pnas.1013391108, 2011.
- 37 Van Der Spoel, D., Lindahl, E., Hess, B., Groenhof, G., Mark, A. E., and Berendsen, H. J. C.:
38 GROMACS: Fast, flexible, and free, *J Comput Chem*, 26, 1701-1718,
39 <https://doi.org/10.1002/jcc.20291>, 2005.
- 40 Wu, C., Wang, C., Wang, S., Wang, W., Yuan, B., Qi, J., Wang, B., Wang, H., Wang, C., Song, W.,
41 Wang, X., Hu, W., Lou, S., Ye, C., Peng, Y., Wang, Z., Huangfu, Y., Xie, Y., Zhu, M., Zheng, J., Wang,
42 X., Jiang, B., Zhang, Z., and Shao, M.: Measurement report: Important contributions of oxygenated
43 compounds to emissions and chemistry of volatile organic compounds in urban air, *Atmos. Chem.*
44 *Phys.*, 20, 14769-14785, 10.5194/acp-20-14769-2020, 2020.
- 45 Wu, H., Li, G., Hou, J., and Sotthewes, K.: Probing surface properties of organic molecular layers by
46 scanning tunneling microscopy, *Adv Colloid Interfac*, 318, 102956,
47 <https://doi.org/10.1016/j.cis.2023.102956>, 2023.



- 1 Xia, S.-Y., Wang, C., Zhu, B., Chen, X., Feng, N., Yu, G.-H., and Huang, X.-F.: Long-term observations
2 of oxygenated volatile organic compounds (OVOCs) in an urban atmosphere in southern China, 2014–
3 2019, *Environ Pollut*, 270, 116301, <https://doi.org/10.1016/j.envpol.2020.116301>, 2021.
- 4 Xu, L., Fukushima, S., Sobanska, S., Murata, K., Naganuma, A., Liu, L., Wang, Y., Niu, H., Shi, Z.,
5 Kojima, T., Zhang, D., and Li, W.: Tracing the evolution of morphology and mixing state of soot
6 particles along with the movement of an Asian dust storm, *Atmos. Chem. Phys.*, 20, 14321-14332,
7 10.5194/acp-20-14321-2020, 2020.
- 8 Zaveri, R. A., Easter, R. C., Shilling, J. E., and Seinfeld, J. H.: Modeling kinetic partitioning of
9 secondary organic aerosol and size distribution dynamics: representing effects of volatility, phase state,
10 and particle-phase reaction, *Atmos. Chem. Phys.*, 14, 5153-5181, 10.5194/acp-14-5153-2014, 2014.
- 11 Zhang, R., Khalizov, A. F., Pagels, J., Zhang, D., Xue, H., and McMurry, P. H.: Variability in
12 morphology, hygroscopicity, and optical properties of soot aerosols during atmospheric processing,
13 *Proceedings of the National Academy of Sciences*, 105, 10291-10296, 10.1073/pnas.0804860105,
14 2008.
- 15